Skeletal muscle-specific T-tubule protein STAC3 mediates voltage-induced Ca^{2+} release and contractility

Benjamin R. Nelson[a], Fenfen Wu[b], Yun Liu[c], Douglas M. Anderson[a], John McAnally[a], Weichun Lin[c], Stephen C. Cannon[b], Rhonda Bassel-Duby[a], and Eric N. Olson[a,1]

Departments of [a]Molecular Biology, [b]Neurology and Neurotherapeutics, and [c]Neuroscience, University of Texas Southwestern Medical Center, Dallas, TX 75390

Contributed by Eric N. Olson, June 4, 2013 (sent for review May 17, 2013)

Excitation–contraction (EC) coupling comprises events in muscle that convert electrical signals to Ca^{2+} transients, which then trigger contraction of the sarcomere. Defects in these processes cause a spectrum of muscle diseases. We report that STAC3, a skeletal muscle-specific protein that localizes to T tubules, is essential for coupling membrane depolarization to Ca^{2+} release from the sarcoplasmic reticulum (SR). Consequently, homozygous deletion of src homology 3 and cysteine rich domain 3 (*Stac3*) in mice results in complete paralysis and perinatal lethality with a range of musculoskeletal defects that reflect a blockade of EC coupling. Muscle contractility and Ca^{2+} release from the SR of cultured myotubes from *Stac3* mutant mice could be restored by application of 4-chloro-*m*-cresol, a ryanodine receptor agonist, indicating that the sarcomeres, SR Ca^{2+} store, and ryanodine receptors are functional in *Stac3* mutant skeletal muscle. These findings reveal a previously uncharacterized, but required, component of the EC coupling machinery of skeletal muscle and introduce a candidate for consideration in myopathic disorders.

dihydropyridine receptor | myopathy | dysgenic | dyspedic | neuromuscular junction

Muscle contraction requires a series of events known as excitation–contraction (EC) coupling that links electrical depolarization, initiated by motor neuron innervation, to muscle contraction by releasing Ca^{2+} from its storage site in the sarcoplasmic reticulum (SR), which consequently activates the sarcomere. In both cardiac and skeletal muscle, this process requires the function of two Ca^{2+} channels, the dihydropyridine receptor (DHPR) and the ryanodine receptor (RyR) (1, 2), but the isoforms of each and the functional relationship between these channels are distinct in each striated muscle tissue.

In cardiac muscle, membrane depolarization results in inward flow of extracellular Ca^{2+} through the DHPR (3). Calcium that enters the cytoplasm through the DHPR then acts as a second messenger upon the RyR, causing the channel to open and release more Ca^{2+} from the SR. By contrast, skeletal muscle does not require extracellular Ca^{2+} to trigger Ca^{2+} release from the SR, and DHPR serves primarily as a voltage sensor (1). The skeletal muscle DHPR does in fact conduct inward Ca^{2+} current, known as L-type current, which is enhanced by retrograde signaling with the RyR (4), but this current is not required for normal EC coupling. Instead, DHPR triggers opening of the RyR in the SR membrane by an unknown physical coupling mechanism, which results in a massive release of Ca^{2+} to activate the sarcomere (2, 4, 5).

The exact coupling mechanism that links the skeletal-type DHPR to the skeletal muscle-specific isoform of RyR (RyR1) has proven difficult to define, although studies using chimeric constructs of skeletal and cardiac DHPR isoforms have successfully mapped the regions that are functionally required for the skeletal-type coupling mechanism (1, 6). There is substantial evidence that the cytoplasmic loop between transmembrane regions II and III (II-III loop) of the DHPR pore-forming subunit (α1s) conveys the skeletal-specific properties of this channel. Whereas the C-terminal portion of the II-III loop has been shown to be sufficient to convey the skeletal muscle-specific properties of the II-III loop (7), other groups have demonstrated that a positively charged portion of the N-terminal region can activate RyR (8, 9), despite the fact that EC coupling was normal when this region was disrupted or deleted (7, 10). Thus, it is unlikely that the N-terminal region of the II-III loop directly activates RyR1 in a normal physiological context. RyR1 has also been shown to be modulated by a variety of accessory proteins including FK506 binding protein 1A (FKBP1A) (11), S100 calcium-binding protein A1 (S100A1) (12), and calmodulin (13).

In a bioinformatic screen for uncharacterized muscle-specific conserved genes with probable function in intracellular signaling, we identified src homology 3 (SH3) and cysteine rich domain 3 (*Stac3*), which we show encodes a skeletal muscle-specific protein that localizes to T tubules. Using a knockout (KO) mouse model and primary myoblast cultures, we demonstrate that STAC3 is required for coupling membrane depolarization to SR Ca^{2+} release and is required for electrically evoked skeletal muscle contraction. Surprisingly, skeletal muscle contractility could be fully restored in the absence of STAC3 by application of the RyR agonist 4-chloro-*m*-cresol (4-CMC). Based on this evidence, we propose that STAC3 may promote coupling between or possibly link the DHPR voltage sensor and the RyR Ca^{2+} release channel. This work expands understanding of EC coupling and may provide insight into Ca^{2+} regulation in other tissues such as the central nervous system, where the related genes *Stac* and *Stac2* are expressed.

Results

Skeletal Muscle-Specific Expression of *Stac3*. STAC3 is a 360-amino acid protein containing a polyglutamic acid region (Poly-E), a domain with similarity to the C1 domain of protein kinase C, and two SH3 protein-interaction domains (Fig. 1*A*). We determined that *Stac3* expression is highly restricted to skeletal muscle throughout development and into adulthood (Fig. 1 and Fig. S1), consistent with in situ hybridization studies in zebrafish (ZFIN Database; http://zfin.org). In contrast, the mouse paralogs *Stac* and *Stac2* are excluded from skeletal muscle but are expressed in a variety of other tissues, including the central nervous system (Fig. 1*B*). *Stac3* expression was absent in myoblasts but robustly

Author contributions: B.R.N., F.W., Y.L., D.M.A., W.L., S.C.C., R.B.-D., and E.N.O. designed research; B.R.N., F.W., Y.L., and D.M.A. performed research; J.M. contributed new reagents/analytic tools; B.R.N., F.W., Y.L., D.M.A., W.L., S.C.C., R.B.-D., and E.N.O. analyzed data; and B.R.N., R.B.-D., and E.N.O. wrote the paper.

The authors declare no conflict of interest.

[1]To whom correspondence should be addressed. E-mail: eric.olson@utsouthwestern.edu.

This article contains supporting information online at www.pnas.org/lookup/suppl/doi:10.1073/pnas.1310571110/-/DCSupplemental.

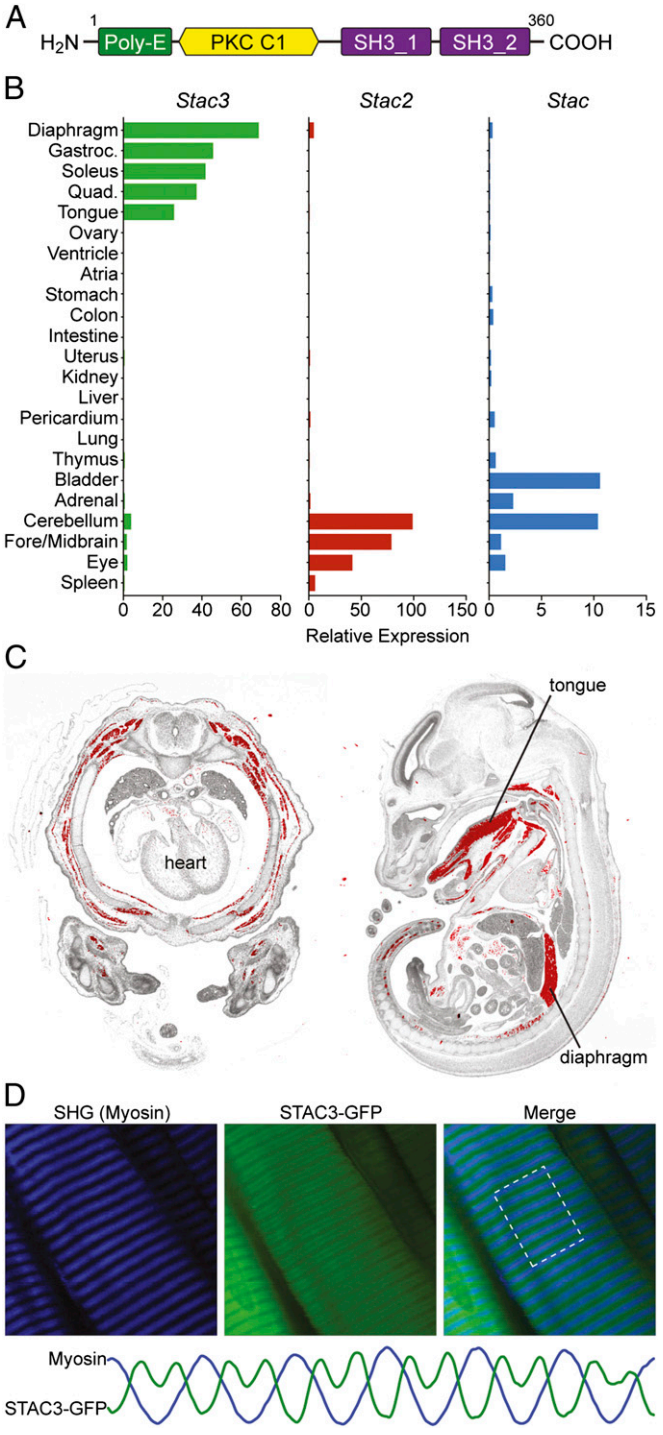

Fig. 1. Domain structure and expression of *Stac3*. (*A*) The domain architecture of STAC3 consists of a region containing 11 consecutive glutamic acid residues (Poly-E), a protein kinase C (PKC) C1 domain, and two SH3 protein-interaction domains. Scales of each domain are not directly proportional. (*B*) Expression profiles of *Stac*, *Stac2*, and *Stac3* determined by real-time PCR in adult mouse tissues. (*C*) In situ hybridization of an E14.5 mouse transverse thorax (*Left*) and an E15.5 sagittal section (*Right*) shows skeletal muscle-specific expression of *Stac3*. Hybridization signal is pseudocolored red. (*D*) T-tubule localization of STAC3. Flexor digitorum brevis muscles were electroporated in vivo with a *Stac3* C-terminal GFP fusion construct, and the live muscle was imaged after a 3-d recovery period. The fusion protein localized in a repeating doublet pattern alternating with the myosin A bands, as visualized by second harmonic generation (SHG). This pattern is consistent with localization to T tubules. The plots for each channel, shown at the bottom, were generated using the ImageJ Plot Profiler tool within the highlighted region. The scales of these plots were arbitrarily adjusted to compare the patterns.

up-regulated upon differentiation of C2C12 myoblasts to myotubes, suggesting a role in mature muscle (Fig. S2). Interestingly, expression of *Stac3* and its related family members is absent in the heart.

Localization of STAC3 to T Tubules. As a first step toward understanding the function of STAC3, we determined the subcellular localization of the protein by electroporating an expression plasmid encoding a fusion protein of STAC3-GFP (GFP at the carboxyl end) into mouse flexor digitorum brevis muscles (FDB) in vivo. Following a 3-d recovery period, the FDB was imaged directly using two-photon laser scanning microscopy with second harmonic generation to visualize the myosin A bands as an internal reference, as described by DiFranco et al. (14). STAC3-GFP localized in a repeating doublet pattern with the wider spaces correlating to the myosin heavy chains (Fig. 1*D*), consistent with a report describing in vivo localization of the T-tubule protein DHPR α1s to the borders of A bands (15). Using this technique, it is not possible to determine whether STAC3 localizes along the full length of the T tubules or more specifically to the triads. Given the critical role of T tubules in EC coupling, localization of STAC3 to these structures is consistent with a role in this process.

Loss of *Stac3* Results in Complete Paralysis and Perinatal Lethality. To further study the expression and function of STAC3 in vivo, we rederived *Stac3* KO mice from germplasm containing a β-galactosidase (LacZ) reporter gene inserted within the first intron of the *Stac3* locus, disrupting expression of the *Stac3* coding sequence (Fig. S3). Expression of the *Stac3*-LacZ allele in heterozygous mice was detected as early as embryonic day 9.5 (E9.5) in somites and was robustly expressed in all fetal and postnatal skeletal muscles (Figs. S4 and S5). In concordance with our expression analysis in wild-type (WT) mice, we did not observe LacZ staining in any tissue other than skeletal muscle as examined by whole-mount staining (Fig. S5).

Mice heterozygous for the LacZ knockin allele were grossly normal in appearance and behavior. In contrast, *Stac3* homozygous KO mice were born with an overall "lunar" shape, characterized by a generally flaccid appearance, wrist drop, and abnormal spinal curvature (Fig. 2*A*). The gross morphology of the KO neonates was similar to that described for mice with severe defects in muscle differentiation (16), neuromuscular junction (NMJ) formation or function (17–19), or EC coupling (20–23). KO neonates were born in expected Mendelian ratios from heterozygous crosses of *Stac3*-LacZ knockin mice, indicating that *Stac3* is not required for embryonic viability (Table S1); however, they were completely paralyzed and died rapidly following birth. Histological examination of KO neonatal lungs revealed that the alveoli were markedly smaller than those in comparable sections of WT lungs (Fig. 2*B*), and KO lungs were not buoyant in saline. Although the mice were paralyzed, the hearts of *Stac3* KOs were observed beating for several minutes following birth. These results suggest that KO mice expire shortly after birth due to hypoxia resulting from the inability to inspire.

Musculoskeletal Defects of *Stac3* KO Mice. To investigate the function of *Stac3*, we examined the musculoskeletal system in KO mice. In comparison with WT mice, the appendicular muscles and diaphragm of *Stac3* KO mice appeared smaller and more translucent. Staining of bone and cartilage revealed that the KO skeletons were abnormally kyphotic, with multiple abnormalities involving the ribs, sternum, and costal cartilages (Fig. 2*C*). KO skeletons also had a dramatic reduction in bone ridge formation at major muscle insertion sites, including the deltoid tuberosity of the humerus and the trochanters of the femurs (Fig. S6). Because bone growth at these sites requires muscle

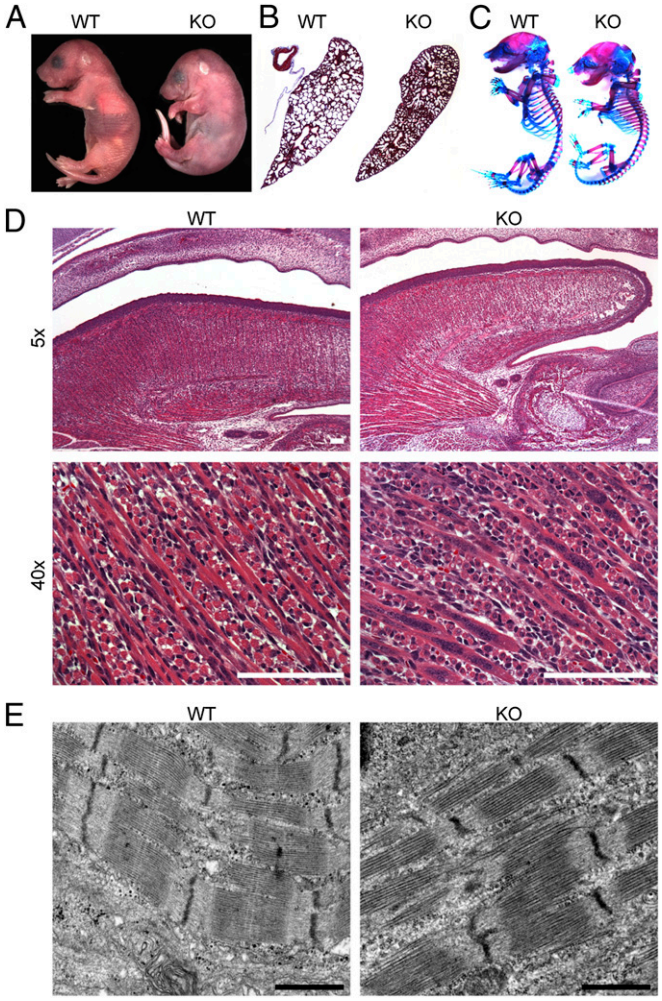

Fig. 2. Abnormalities of *Stac3* KO mice. (*A*) Complete paralysis, wrist drop, and abnormally rounded lunar appearance of a newborn *Stac3* KO mouse. (*B*) Alveoli of KO lungs are not inflated, as shown by Masson's trichrome staining. (*C*) Whole-mount E18.5 skeletons prepared with alcian blue, a cartilage stain, and alizarin red S, a bone stain, show numerous abnormalities in KOs, including abnormal spinal curvature, growth defects in costal cartilages, and decreased bone formation at muscle insertion sites. (*D*) H&E sagittal paraffin sections of E16.5 heads show decreased muscle mass of the tongue and abnormal clustering of nuclei in KOs. KO fibers also have fewer observable striations, and most have a vacuolated appearance. (*E*) Electron microscopy of E15.5 tongues shows that sarcomeres are present in KO fibers as seen here but overall, sarcomeres appear more disorganized (Fig. S7). (Scale bars, 1 μm.)

development and function, this evidence supports the conclusion that KO mice are paralyzed throughout development (24).

Based on the striking similarity between *Stac3* KO mice and other paralytic muscle phenotypes, we hypothesized that *Stac3* may be critical for muscle differentiation, NMJ formation, or EC coupling. Fundamental defects in muscle differentiation could be ruled out because skeletal muscle was formed in KO mice, albeit with reduced mass and aberrant morphology (Fig. 2*D*). Myofibers from KO mice were clearly multinucleated in H&E sections, but the nuclei were typically seen clustered together instead of being distributed uniformly along the fiber as in normal muscle. Myonuclei of KO fibers also failed to migrate to the periphery of the fibers by E18.5, compared with WT muscle. Whereas striations were rarely observed in some regions of the KO muscle, visualized by H&E staining, overall the fibers appeared mottled and vacuolated. Transmission electron microscopy of tongue muscle demonstrated myofibril formation, although there were obvious signs of structural heterogeneity and disorganization in the KO (Fig. 2*E* and Fig. S7). In culture, primary myoblasts isolated from E18.5 forelimbs and hindlimbs of KO fetuses differentiated and fused normally, yielding multinucleated myotubes. However, differentiated KO myotubes never spontaneously twitched, as observed in cultures of normal myotubes. We conclude that although there are clear defects in muscle maturation, mass, and morphology, myoblast differentiation or fusion can occur in the absence of STAC3.

Neuromuscular Junctions Are Functional in *Stac3* KO Mice. To determine whether the absence of STAC3 disrupts NMJ formation or function, we labeled acetylcholine receptors of E18.5 diaphragms with Texas red α-bungarotoxin and the phrenic nerve with an antibody against syntaxin (Fig. 3). In the *Stac3* KO muscles, we found that NMJs were properly formed, with the nerve terminals directly apposing acetylcholine receptor clusters of the muscle (Fig. 3*B*). However, there was increased branching of the phrenic nerve and a slightly broader spatial distribution of the NMJs (Fig. 3*A*), both of which are features that were previously described in mice lacking key components of EC coupling (25–27). Interestingly, E18.5 KO diaphragms displayed an increase in miniature end-plate potentials (Fig. 4), a feature reported previously with loss of EC coupling components (25). We observed normal evoked end-plate potentials following electrical stimulation of the phrenic nerve (Fig. 4 *C* and *D*). Muscle action potentials were also comparable in WT and KO mice, but the action potentials failed to induce contraction in the KO muscles (Fig. 4*E*). These experiments demonstrate that STAC3 is not required for synaptic transmission or development of the NMJ, nor is it required for action potential generation or propagation. Because no contraction was observed in response to muscle action potentials evoked by nerve stimulation, the defect in the KO muscle must lie downstream of excitation.

Lack of Depolarization-Evoked Contraction in the Absence of STAC3. To further examine the mechanistic basis for the lack of electrically induced contraction in *Stac3* KO muscle, we conducted muscle contraction assays on dissected diaphragms from E18.5 embryos. Indeed, electrical field stimulation of WT or heterozygous (Het) diaphragms triggered robust contractions at all tested frequencies, but contractions of the KO diaphragms were barely detectable (Fig. 5*A*). We tested whether addition of the RyR agonist 4-CMC could induce contraction, and found that 4-CMC–induced contractions in normal and KO diaphragms generated approximately the same magnitude of force when normalized for differences in muscle weight. Diaphragms from the KO mice were also insensitive to membrane depolarization with potassium chloride (Fig. 5*B*). These results indicate that SR Ca^{2+} stores in the KO muscles are adequate for contraction and that the contractile apparatus functions normally, despite the disorganization observed by histology and electron microscopy. Therefore, these abnormalities likely arise secondarily to complete lack of muscle function in the absence of STAC3.

***Stac3* KO Myotubes Lack Depolarization-Induced Ca^{2+} Transients.** From the muscle contraction experiments, we concluded that loss of *Stac3* likely blocks voltage-induced Ca^{2+} release from the SR. To test this hypothesis directly, we isolated myoblasts from E18.5 embryos and differentiated them in vitro. Next, we loaded normal and KO myotubes with the fluorescent Ca^{2+} indicator fluo-4-AM and imaged these cells during depolarization with KCl and stimulation with 4-CMC. In the absence of stimulation, we found spontaneous twitch-associated Ca^{2+} transients in WT and Het myotubes, but no spontaneous Ca^{2+} transients were seen in KO myotubes (Fig. 5*C* and Movies S1 and S2). Occasionally, we observed slowly propagating waves of Ca^{2+} in KO myotubes, but never rapid, synchronous transients involving the

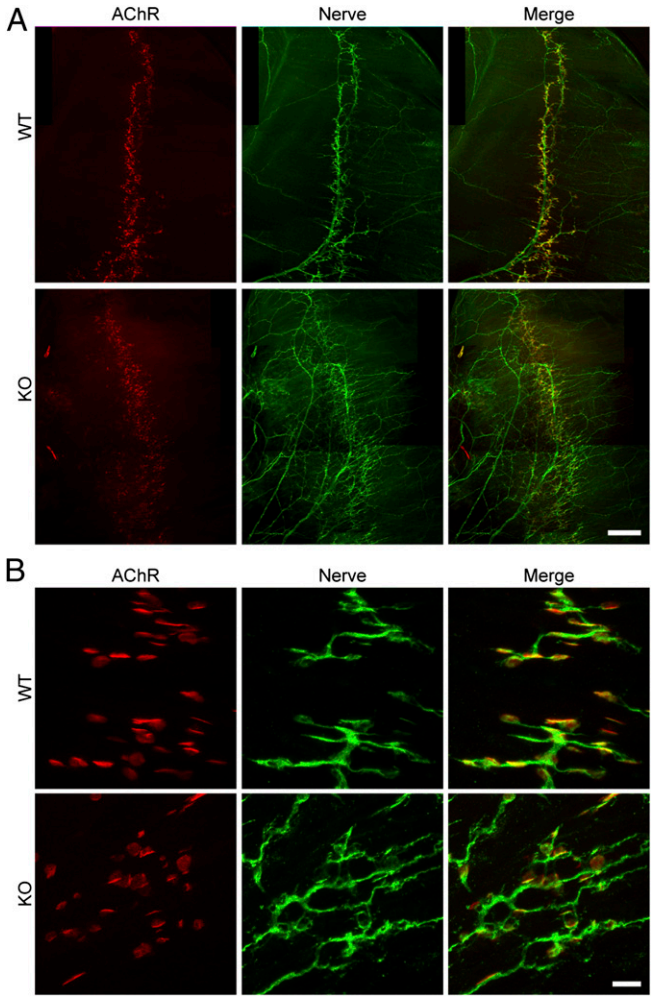

Fig. 3. Normal NMJ formation but increased nerve branching in KO mice. Whole mounts of E18.5 diaphragm muscles were double-stained with Texas red α-bungarotoxin to label postsynaptic AChRs and an antibody against syntaxin to label presynaptic nerves. In both WT and KO muscles, presynaptic nerve terminals formed in juxtaposition with postsynaptic AChR clusters (*B*). However, there were increased nerve branching and defasciculation in the KO diaphragm compared with the WT (*A*). AChR clusters also occupied a broader area in the central region of the KO diaphragm. [Scale bars, 400 μm (*A*), 20 μm (*B*).]

entire myotube. Application of 120 mM KCl to WT or Het myotubes caused massive synchronous Ca^{2+} transients, whereas KO myotubes were unresponsive; however, Het and KO myotubes responded similarly to application of 4-CMC. These experiments demonstrate that the complete paralysis seen in *Stac3* KO mice results from a defect in voltage-induced Ca^{2+} release from the SR.

Expression of Known EC Coupling Components in *Stac3* KO Muscle. Collectively, our data reveal a previously unrecognized but essential role for STAC3 in voltage-induced Ca^{2+} release and consequently skeletal muscle contraction. This phenomenon may result from reduced expression or mislocalization of DHPR or RyR1, but we found that mRNA levels of these components are similar in WT and KO muscles (Fig. S8*A*) and that KO muscles responded normally to 4-CMC, indicating normal RyR function (Fig. 5*C* and Fig. S9). Protein levels of DHPR α1s and RyR1 were decreased, but not absent, in tongue muscle of KO compared with WT mice at E18.5 (Fig. S8*B*). In primary myotube cultures, we found that expression of these components was slightly increased in the KO above those of Het myotubes, suggesting that there may be compensation in these cells or that the expression of these components in embryonic muscle may be dependent upon muscle use.

Discussion

The results of this study identify STAC3 as a previously unrecognized regulator of skeletal muscle contraction and demonstrate that STAC3 is required for voltage-induced Ca^{2+} release from the SR. Although the exact mechanism by which STAC3 functions in this process is still unknown, our results suggest that it is functionally involved in the coupling of voltage changes in the plasma membrane to Ca^{2+} release from the SR.

While this work was being completed, two other reports described the requirement of *Stac3* for skeletal muscle function, but the mechanistic basis of its role was unclear. Bower et al. reported that *Stac3* is required for myotube formation and differentiation of skeletal myoblasts in zebrafish, based on morpholino knockdown studies in zebrafish embryos and RNAi in cultured C2C12 mouse myoblasts (28). In contrast, our results clearly demonstrate that *Stac3* is not required for myofiber formation in mice, and that myoblasts from *Stac3* KO mice differentiate in culture. Reinholt et al. described the lethal skeletal muscle phenotype of mice with the same insertional mutation analyzed in our studies (29). They concluded that *Stac3* was required for correct subcellular localization of myonuclei and also that *Stac3* KO mice may have increased myoblast fusion. Although myofibers from *Stac3* KO mice are dysmorphic, our

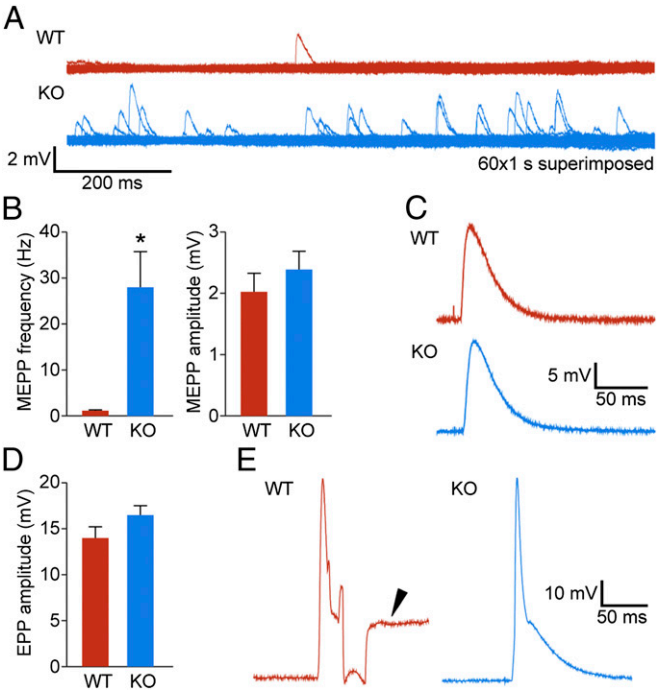

Fig. 4. Increased neuromuscular synaptic activity. (*A*) Examples of miniature end-plate potential (mEPP) traces obtained from 1-min continuous recording (superimposed traces are shown; 60×, 1-s). mEPP frequencies were significantly increased in E18.5 KO mice compared with WT. (*B*) Quantification of mEPP frequencies and amplitudes. Frequency: KO (27.99 ± 7.73 events per min, $n = 22$ cells), WT (1.15 ± 0.13 events per min, $n = 13$ cells), $^*P < 0.05$; mEPP amplitude (no statistical difference): KO (2.4 ± 0.3 mV, $n = 22$ cells), WT (2.04 ± 0.3 mV, $n = 13$ cells). (*C*) Sample traces of end-plate potentials. (*D*) Quantification of EPP amplitudes (no statistical difference): WT (14 ± 1.44 mV, $n = 9$ cells) and KO (16.46 ± 1.01 mV, $n = 16$ cells). Statistical data are represented as mean ± SEM. (*E*) Traces of muscle action potentials are comparable in WT and KO. The arrowhead indicates a contraction artifact, which was not observed in KO muscles due to their paralysis.

results suggest that this defect, as well as abnormalities in subcellular structure, result secondarily from the complete absence of muscle contractility, rather than from a primary role of STAC3 in these processes. Indeed, our finding that *Stac3* KO muscle is unresponsive to depolarization, but that contraction can be rescued by exposure to the RyR agonist 4-CMC, demonstrates that the primary defect in these mice is the complete loss of voltage-dependent Ca^{2+} release from the SR. Thus, we can only conclude that other abnormalities result primarily from lack of Ca^{2+} transients or contraction.

We found that loss of *Stac3* in muscle results in non-autonomous effects on the skeleton and motor neurons. Although this pattern of defects is known to result from loss of EC coupling, the underlying mechanisms are still somewhat vague. Skeletal defects have been hypothesized to result from lack of mechanical stimulation of bone and maintenance of posture in utero (24). Increased phrenic nerve branching and miniature end-plate potentials have been shown in other EC coupling null mutants, including muscular dysgenesis (DHPR α1s null), DHPR β1 null, and RyR1 null mice. The exact cause of this phenomenon is unclear, but it demonstrates the interdependence of muscle and motor neuron development and the importance of EC coupling in these processes.

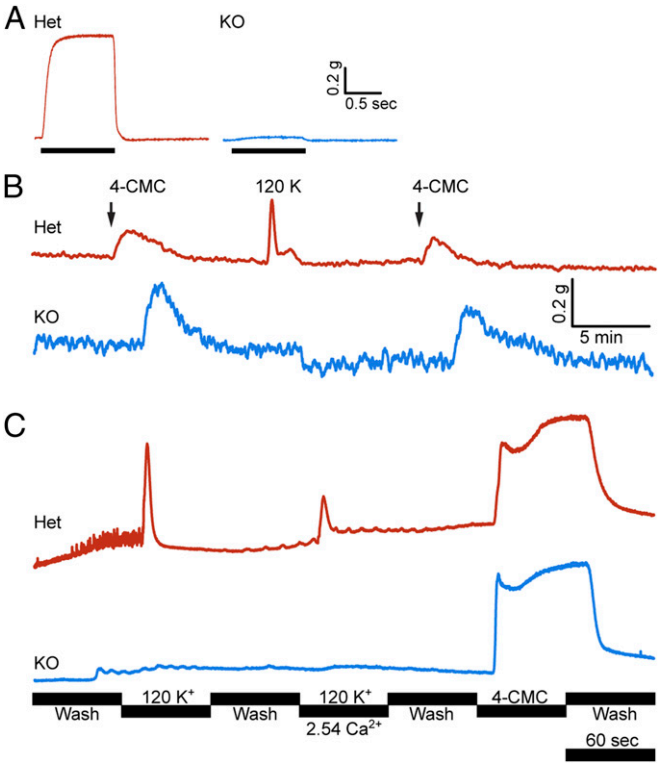

Fig. 5. Muscle contraction and calcium transients. (*A*) Contraction of E18.5 diaphragm was elicited by electrical field stimulation (50 Hz, 1-ms pulses) and measured with a force transducer. Stimulation yielded robust tetanic contraction in normal diaphragms, but barely detectable contraction in KOs. (*B*) Force measurements of diaphragm with application of 120 mM KCl and 1 mM 4-CMC. Het and KO responded comparably to 4-CMC when normalized for differences in weight, but the KO tissue was unresponsive to membrane depolarization by KCl. The amplitudes of the traces in *A* and *B* were normalized to the specimen weight. (*C*) Cultured myotubes loaded with the fluorescent calcium indicator fluo-4-AM. The cells were perfused continuously and the calcium transients were recorded with an inverted microscope. Het cells responded synchronously to KCl application and to 4-CMC. KO myotubes were unresponsive to KCl, but responded comparably with Het with application of 4-CMC. Each fluo-4-AM trace is the mean of ~10 myotubes within the field.

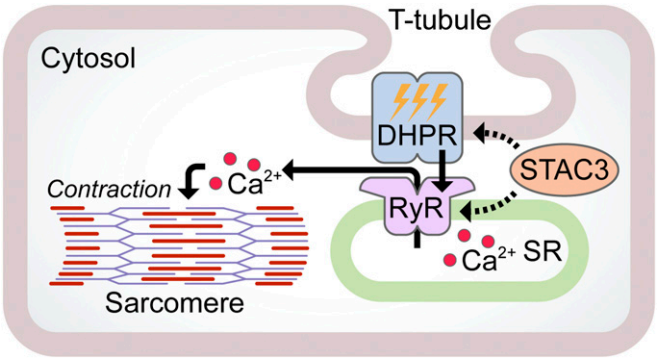

Fig. 6. Hypothetical model of STAC3 function. Upon activation of DHPR by an action potential, a conformational change is transmitted to RyR in the SR membrane, resulting in SR calcium release and sarcomere contraction. STAC3 may facilitate this process by interaction with DHPR, RyR, or both.

Because STAC3 is a skeletal muscle-specific protein with no paralog in cardiac muscle, it is likely that it specifically facilitates skeletal-type EC coupling. To do this, STAC3 may act upon either DHPR or RyR to facilitate their activation or localization (Fig. 6). Accordingly, STAC3 may be involved in the formation, trafficking, or stability of the DHPR complex or the formation of tetrads, the skeletal muscle-specific Ca^{2+} release units. Another possibility is that STAC3 may directly couple DHPR to RyR1 by a conformation-dependent mechanism, because these channels have long been known to physically interact, but conclusive evidence of direct interaction has been elusive. Further work will be necessary to fully elucidate the function of STAC3 in regard to its possible molecular interactions with other EC coupling components. Although STAC3 is required for voltage-induced Ca^{2+} release in skeletal muscle, there may still be unknown proteins that are required for this process with which STAC3 might interact.

Because mutations in other EC coupling components are known to cause muscle diseases, it is expected that mutations in *Stac3* likely cause disease as well. Identification of individuals with hypomorphic or gain-of-function mutations in *Stac3* could be instrumental in understanding the function of this gene. For instance, are there mutations in *Stac3* that result in altered RyR1 gating, possibly resulting in susceptibility to malignant hyperthermia, nemaline myopathy, central core disease, or multiminicore disease? It would also be interesting to know whether *Stac* or *Stac2* can rescue the KO myotubes and whether chimeras between *Stac3* and these genes might be useful study tools. Finally, it would be interesting to explore whether *Stac3* paralogs may be involved in Ca^{2+} signaling in their respective tissues.

Materials and Methods

Mice. All experiments involving animals were approved by the Institutional Animal Care and Use Committee at the University of Texas Southwestern Medical Center. The *Stac3* knockout strain was rederived on a mixed background by in vitro fertilization using germplasm stock obtained from the National Institutes of Health Knock-Out Mouse Project (KOMP; www.komp.org; Project ID CSD41137).

Muscle Electroporation and Imaging. Flexor digitorum brevis muscles were electroporated following a published protocol (14). Following a 3-d recovery, the mice were killed, their feet were skinned, and the unfixed FDB was examined directly in imaging buffer by two-photon laser scanning microscopy (Zeiss; LSM 780) with reverse second harmonic generation to visualize the A bands as an internal reference.

Electrophysiology. Measurement of neuromuscular synaptic and muscle activity was carried out on acutely isolated E18.5 phrenic nerve-diaphragm muscle preparations, as previously described (30). A detailed description is available in *SI Materials and Methods*.

Contraction Assays. Diaphragm contraction assays were carried out as described previously (31, 32). A detailed description is available in *SI Materials and Methods*.

Ca^{2+} Measurements. Primary myoblasts were differentiated for 6 d and then loaded with the fluorescent Ca^{2+} indicator fluo-4-AM. Calcium transients were recorded using an Applied Precision DeltaVision pDV microscope with a 20× objective, FITC filters, and a heated chamber. Medium was continuously perfused in a closed-bath perfusion chamber. The perfusion buffers were as follows: Ca^{2+}-free Ringer's solution wash, Ca^{2+}-free high-K^+ Ringer's solution, high-K^+ Ringer's solution, or Ca^{2+}-free Ringer's solution with 1 mM 4-CMC. Each treatment lasted 1 min. *z*-axis plots were generated using ImageJ (33) by selecting the outlines of ∼10 myotubes. *z*-axis plots for background regions were also calculated and subtracted from the myotube signal to yield the corrected value.

Detailed methods for all experiments are available in *SI Materials and Methods*.

ACKNOWLEDGMENTS. We are grateful to Dr. Douglas Millay for scientific discussions, Dr. Dennis Burns for discussions on EM images, Jose Cabrera for graphics, and Drs. Susan Hamilton and Leslie Leinwand for helpful comments on the paper. We thank Abhijit Bugde and Dr. Kate Luby-Phelps for assistance and helpful advice at the Live Cell Imaging Core Facility at University of Texas (UT) Southwestern, John Shelton for help with histology and imaging, and Dr. Karen Rothberg at the UT Southwestern Electron Microscopy Core Facility. We also thank the National Institutes of Health (NIH) KOMP for providing the *Stac3* KO germplasm. This work was supported by NIHGrants HL-077439, HL-111665, HL-093039, U01-HL-100401, and AR-063182; and The Welch Foundation Grant 1-0025 (to E.N.O.). B.R.N. is supported by NIH training Grant T32-HL-007360.

1. Tanabe T, Beam KG, Adams BA, Niidome T, Numa S (1990) Regions of the skeletal muscle dihydropyridine receptor critical for excitation-contraction coupling. *Nature* 346(6284):567–569.
2. Block BA, Imagawa T, Campbell KP, Franzini-Armstrong C (1988) Structural evidence for direct interaction between the molecular components of the transverse tubule/sarcoplasmic reticulum junction in skeletal muscle. *J Cell Biol* 107(6 Pt 2):2587–2600.
3. Bers DM (2002) Cardiac excitation-contraction coupling. *Nature* 415(6868):198–205.
4. Nakai J, et al. (1996) Enhanced dihydropyridine receptor channel activity in the presence of ryanodine receptor. *Nature* 380(6569):72–75.
5. Paolini C, Fessenden JD, Pessah IN, Franzini-Armstrong C (2004) Evidence for conformational coupling between two calcium channels. *Proc Natl Acad Sci USA* 101 (34):12748–12752.
6. Kugler G, Weiss RG, Flucher BE, Grabner M (2004) Structural requirements of the dihydropyridine receptor alpha1S II-III loop for skeletal-type excitation-contraction coupling. *J Biol Chem* 279(6):4721–4728.
7. Wilkens CM, Kasielke N, Flucher BE, Beam KG, Grabner M (2001) Excitation–contraction coupling is unaffected by drastic alteration of the sequence surrounding residues L720–L764 of the alpha1S II-III loop. *Proc Natl Acad Sci USA* 98(10):5892–5897.
8. El-Hayek R, Ikemoto N (1998) Identification of the minimum essential region in the II-III loop of the dihydropyridine receptor alpha 1 subunit required for activation of skeletal muscle-type excitation-contraction coupling. *Biochemistry* 37(19):7015–7020.
9. Leong P, MacLennan DH (1998) A 37-amino acid sequence in the skeletal muscle ryanodine receptor interacts with the cytoplasmic loop between domains II and III in the skeletal muscle dihydropyridine receptor. *J Biol Chem* 273(14):7791–7794.
10. Bannister RA, Papadopoulos S, Haarmann CS, Beam KG (2009) Effects of inserting fluorescent proteins into the alpha1S II-III loop: Insights into excitation-contraction coupling. *J Gen Physiol* 134(1):35–51.
11. Avila G, Lee EH, Perez CF, Allen PD, Dirksen RT (2003) FKBP12 binding to RyR1 modulates excitation-contraction coupling in mouse skeletal myotubes. *J Biol Chem* 278(25):22600–22608.
12. Prosser BL, et al. (2008) S100A1 binds to the calmodulin-binding site of ryanodine receptor and modulates skeletal muscle excitation-contraction coupling. *J Biol Chem* 283(8):5046–5057.
13. Rodney GG, Williams BY, Strasburg GM, Beckingham K, Hamilton SL (2000) Regulation of RYR1 activity by Ca(2+) and calmodulin. *Biochemistry* 39(26):7807–7812.
14. DiFranco M, Quinonez M, Capote J, Vergara J (2009) DNA transfection of mammalian skeletal muscles using in vivo electroporation. *J Vis Exp* (32), 10.3791/1520.
15. DiFranco M, Tran P, Quiñonez M, Vergara JL (2011) Functional expression of transgenic 1sDHPR channels in adult mammalian skeletal muscle fibres. *J Physiol* 589(Pt 6): 1421–1442.
16. Hasty P, et al. (1993) Muscle deficiency and neonatal death in mice with a targeted mutation in the myogenin gene. *Nature* 364(6437):501–506.
17. Brandon EP, et al. (2003) Aberrant patterning of neuromuscular synapses in choline acetyltransferase-deficient mice. *J Neurosci* 23(2):539–549.
18. DeChiara TM, et al. (1996) The receptor tyrosine kinase MuSK is required for neuromuscular junction formation in vivo. *Cell* 85(4):501–512.
19. An MC, et al. (2010) Acetylcholine negatively regulates development of the neuromuscular junction through distinct cellular mechanisms. *Proc Natl Acad Sci USA* 107(23):10702–10707.
20. Pai AC (1965) Developmental genetics of a lethal mutation, muscular dysgenesis (Mdg), in the mouse. I. Genetic analysis and gross morphology. *Dev Biol* 11:82–92.
21. Takeshima H, et al. (1994) Excitation-contraction uncoupling and muscular degeneration in mice lacking functional skeletal muscle ryanodine-receptor gene. *Nature* 369(6481):556–559.
22. Gregg RG, et al. (1996) Absence of the beta subunit (cchb1) of the skeletal muscle dihydropyridine receptor alters expression of the alpha 1 subunit and eliminates excitation-contraction coupling. *Proc Natl Acad Sci USA* 93(24):13961–13966.
23. Zvaritch E, et al. (2007) An Ryr1I4895T mutation abolishes Ca^{2+} release channel function and delays development in homozygous offspring of a mutant mouse line. *Proc Natl Acad Sci USA* 104(47):18537–18542.
24. Blitz E, et al. (2009) Bone ridge patterning during musculoskeletal assembly is mediated through SCX regulation of Bmp4 at the tendon-skeleton junction. *Dev Cell* 17(6):861–873.
25. Chen F, et al. (2011) Neuromuscular synaptic patterning requires the function of skeletal muscle dihydropyridine receptors. *Nat Neurosci* 14(5):570–577.
26. Powell JA, Rieger F, Blondet B, Dreyfus P, Pinçon-Raymond M (1984) Distribution and quantification of ACh receptors and innervation in diaphragm muscle of normal and mdg mouse embryos. *Dev Biol* 101(1):168–180.
27. Rieger F, Powell JA, Pinçon-Raymond M (1984) Extensive nerve overgrowth and paucity of the tailed asymmetric form (16 S) of acetylcholinesterase in the developing skeletal neuromuscular system of the dysgenic (mdg/mdg) mouse. *Dev Biol* 101(1): 181–191.
28. Bower NI, et al. (2012) Stac3 is required for myotube formation and myogenic differentiation in vertebrate skeletal muscle. *J Biol Chem* 287(52):43936–43949.
29. Reinholt BM, Ge X, Cong X, Gerrard DE, Jiang H (2013) Stac3 is a novel regulator of skeletal muscle development in mice. *PLoS One* 8(4):e62760.
30. Liu Y, et al. (2008) Essential roles of the acetylcholine receptor gamma-subunit in neuromuscular synaptic patterning. *Development* 135(11):1957–1967.
31. Martin-Caraballo M, Campagnaro PA, Gao Y, Greer JJ (2000) Contractile and fatigue properties of the rat diaphragm musculature during the perinatal period. *J Appl Physiol* 88(2):573–580.
32. Wu F, et al. (2011) A sodium channel knockin mutant (NaV1.4-R669H) mouse model of hypokalemic periodic paralysis. *J Clin Invest* 121(10):4082–4094.
33. Schneider CA, Rasband WS, Eliceiri KW (2012) NIH Image to ImageJ: 25 years of image analysis. *Nat Methods* 9(7):671–675.